ACS APPLIED ENERGY MATERIALS

www.acsaem.org

Article

The Importance of Conserving the Stoichiometry of Wide-Bandgap Perovskites in Additive Engineering

Nick R. M. Schipper, Guus J. W. Aalbers, Laura Bellini, Simon V. Quiroz Monnens, Lana M. Kessels, Junke Wang, Martijn M. Wienk, and René A. J. Janssen*

Cite This: ACS Appl. Energy Mater. 2025, 8, 14486−14497

Read Online

ACCESS | Metrics & More | Article Recommendations | Supporting Information

ABSTRACT: Additive engineering is among the most commonly used strategies to enhance the performance and stability of perovskite solar cells. Prior research often focused on optimizing device performance by using additives in the perovskite precursor solution to influence the rate of crystallization and film formation, but a fundamental understanding of the effect of additives on the stoichiometry of the absorber remains elusive. In this study, we reveal how additives affect the ABX_3 stoichiometry of the perovskite absorber and its photovoltaic properties. We find that the solar cell performance of a wide-bandgap (1.77 eV) $Cs_{0.2}FA_{0.8}Pb(I_{0.6}Br_{0.4})_3$ perovskite decreases when processed with either of two common additives, lead thiocyanate and lead chloride, because the additive disturbs the stoichiometry. Interestingly, the addition of excess formamidinium iodide (FAI) to the precursor solution can restore the initial ABX_3 stoichiometry and fully recover the device performance. The excess of FAI that is required depends on whether the halide or pseudohalide additive is incorporated into the crystal lattice. Finally, we alter the stoichiometry of an additive-free perovskite absorber by inducing either an excess or a deficiency of FAI or lead iodide in the precursor and show that slight deviations from the ideal stoichiometry rapidly degrade the device performance. This work provides fundamental insights into the importance of bulk stoichiometry in perovskite absorbers and can serve as a basis for future rational additive engineering.

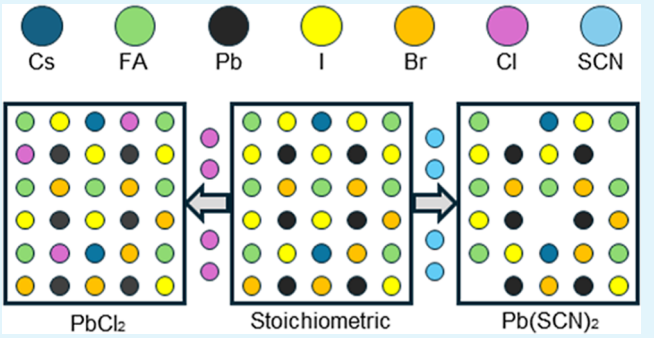

KEYWORDS: *perovskite, stoichiometry, additive engineering, solar cells, device performance*

1. INTRODUCTION

Metal-halide perovskite solar cells have gained significant interest over the past decade, leading to a rapid increase of power conversion efficiency (PCE) from 3.8% for single-junction solar cells in 2009 to 34.85% for a perovskite-on-silicon tandem solar cell in 2025.[1,2] Metal-halide perovskites are semiconductors with an ABX_3 stoichiometry, in which A is a monovalent cation, such as formamidinium (FA^+), cesium (Cs^+), or methylammonium (MA^+), B is a bivalent metal cation such as lead (Pb^{2+}) or tin (Sn^{2+}), and X is a monovalent halide anion, i.e., iodide (I^-), bromide (Br^-), or chloride (Cl^-). By changing the chemical composition, the bandgap of metal-halide perovskites can be varied over a wide range, making them of special interest for multijunction solar cells. In these architectures, multiple absorbers with cascaded bandgaps are stacked and tuned to specific regions of the solar spectrum to reduce thermalization and absorption losses.[3]

Despite their potential and efforts aimed at improving the performance of single-junction perovskite solar cells to approach the Shockley−Queisser limit,[4] metal-halide perovskites remain prone to conversion losses due to defects. Shallow defects located close to either the valence or conduction band act as temporary charge carrier trapping centers,[5] while deep defects located in the middle of the bandgap are effective centers for charge carrier recombination.[6] Defect states in the bulk or at interfaces contribute significantly to nonradiative charge recombination and are thus directly related to losses in open-circuit voltage (V_{oc}). Examples of these defects include halide vacancies,[7] interstitials,[8] and antisites,[9] but also grain boundaries can have a significant effect on the losses in a solar cell.[10] These effects become much more significant when increasing the bandgap of the solar cell by replacing I^- with Br^- because the crystallization dynamics and formation energy of iodide- and bromide-rich perovskites differ significantly, for example leading to wrinkled films and halide segregation.[11]

Received: July 18, 2025
Revised: August 25, 2025
Accepted: September 5, 2025
Published: September 17, 2025

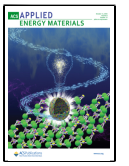

In an effort to eliminate these defects, optimization strategies are employed that target either the perovskite bulk or adjacent interfaces. Examples include strain and lattice engineering,[12] interface engineering,[13] compositional engineering,[14] and additive engineering,[15−18] of which especially the latter has gained significant interest in recent years, due to a wide variety of additives that can enhance device performance.

Previously, Nguyen et al. showed that adding 2 mol % of lead thiocyanate ($Pb(SCN)_2$) into a 1.87 eV $Cs_{0.1}FA_{0.9}PbI_{1.4}Br_{1.6}$ perovskite precursor solution results in a 16-fold increase in grain size, accompanied by higher photoluminescence quantum yield due to a decrease in nonradiative recombination.[19] The authors provided two parts of additional formamidinium iodide (FAI) per part of $Pb(SCN)_2$ to compensate for the FAI that is consumed while forming volatile formamidine and thiocyanic acid. Similar effects on the grain size were observed by Ke et al. in a 1.57 eV $MAPbI_3$ composition, where 5 mol % of $Pb(SCN)_2$ resulted in a significant increase of the average grain size of up to 20 times, but without compensating with additional FAI.[20] Likewise, lead thiocyanate has been found to increase surface uniformity and grain size in a tin-based $FASnI_3$ perovskite.[21]

Lead chloride ($PbCl_2$) is another commonly used additive, which is reported to retard perovskite crystallization and improve the crystallinity by forming an intermediate $MAPbCl_3$ phase in $MAPbI_3$ perovskites, and therewith suppresses charge recombination and enhances charge extraction.[22,23] Furthermore, Zhang et al. showed that adding 10 mol % of $PbCl_2$ into a $MAPbI_3$ perovskite improves the perovskite film quality and significantly increases the grain size.[24]

While these prior studies report the beneficial effect on crystallinity and grain size by incorporating $Pb(SCN)_2$ or $PbCl_2$ in the perovskite precursor solution, the role of these additives in the final film is less clear. In the present study, we propose that a universal mechanism governs lead-based additive engineering, which we ascribe to their capability to disturb the ABX_3 stoichiometry of the perovskite absorber, depending on whether the halide or pseudohalide remains in the film after thermal annealing. We employ two commonly used additives, $Pb(SCN)_2$ and $PbCl_2$, when forming a wide-bandgap (1.77 eV) $Cs_{0.2}FA_{0.8}Pb(I_{0.6}Br_{0.4})_3$ perovskite. This bandgap is ideal for high-performing all-perovskite tandem solar cells, and serves as a model for a range of modern mixed-cation mixed-halide perovskites.[25] Furthermore, this perovskite composition consists of most of the commonly used A- and X-site ions within lead-based perovskites. This broadens the applicability of this study to a wider range of compositions that contain the same components. We show that the ability of these additives to alter the stoichiometry of the perovskite bulk leads to significant reduction of device performance. Subsequently, we combine the additives with additional FAI to restore the stoichiometry to the precise ABX_3 composition and demonstrate that this leads to a full recovery of device performance. The amount of FAI that is required to restore the stoichiometry depends on whether the additive is built into the perovskite lattice. Hence, for $PbCl_2$ one equivalent of FAI is needed because chloride is built into the perovskite lattice, but for $Pb(SCN)_2$ three equivalents of FAI are required because thiocyanate is not incorporated into the perovskite. To support these results, we show that disturbing the stoichiometry of an additive-free perovskite absorber results in similar changes in performance. We conclude that maintaining the bulk stoichiometry of perovskites during material optimization is essential for understanding the intrinsic effects of lead-based additives on the performance of perovskite solar cells.

2. EXPERIMENTAL SECTION

2.1. Materials. Unless mentioned otherwise, all materials were used as received without purification and stored under an inert atmosphere. Lead bromide ($PbBr_2$, >98%), lead iodide (PbI_2, 99.99%, trace metal basis), lead chloride ($PbCl_2$, >99%), lead thiocyanate ($Pb(SCN)_2$, >98%), [4-(3,6-dimethyl-9H-carbazol-9-yl)butyl]-phosphonic acid (Me-4PACz, >98%), and 1,6-hexylene diphosphonic acid (HDPA, >98%) were purchased from TCI chemicals. Formamidinium iodide (FAI, >99.99%) and propane-1,3-diammonium iodide ($PDAI_2$) were purchased from Greatcell Solar Materials. Cesium iodide beads (CsI, 99.999%) and aluminum oxide nanoparticles (Al_2O_3, 20 wt % in IPA) were purchased from Sigma-Aldrich. Phenyl-C_{61}-butyric acid methyl ester (PCBM, 99%) was purchased from Solenne BV. Nickel oxide nanoparticle ink (NiO_x, 2.5 wt % in ethanol) was purchased from Avantama. Bathocuproine (BCP, >99.5%) was purchased from Lumtec. Dimethylformamide (DMF, anhydrous 99.9%), dimethyl sulfoxide (DMSO, anhydrous 99.9%), anisole (anhydrous 99.7%), propan-2-ol (IPA, anhydrous, 99.95%), and chlorobenzene (CB, anhydrous 99.8%) were purchased from Sigma-Aldrich. Ethanol (EtOH, > anhydrous 95%) and dodecyl sodium sulfate (99%) were purchased from Acros Organics.

2.2. Solution Preparation. All solutions were prepared and spin coated in a N_2-filled glovebox. A stoichiometric $Cs_{0.2}FA_{0.8}Pb(I_{0.6}Br_{0.4})_3$ perovskite solution (1.2 M) was prepared by dissolving PbI_2 (221.3 mg, 0.48 mmol), $PbBr_2$ (264.3 mg, 0.72 mmol), FAI (165.1 mg, 0.96 mmol) and CsI (62.4 mg, 0.24 mmol) in 1 mL of DMF/DMSO 4:1 (v/v). For additive-containing solutions, 0.5−2 mol % of $PbCl_2$ or $Pb(SCN)_2$ was added to the precursor solution, alongside with 0−4 mol % of FAI. For nonstoichiometric precursors, 1−4 mol % of either FAI or PbI_2 was added to or removed from the precursor. The precursor solution was stirred at 60 °C for 60 min and cooled to room temperature prior to deposition. The NiO_x nanoparticle dispersion was prepared by diluting the NiO_x nanoparticle ink with EtOH at a ratio of NiO_x/EtOH 1:10 (v/v). Me-4PACz was dissolved in EtOH (0.5 mg mL^{-1}). The commercial Al_2O_3 nanoparticle dispersion (20 wt % in IPA) was diluted with IPA in a 1:150 (v/v) ratio. For top passivation, $PDAI_2$ was dissolved in a mixture of IPA/CB 2:1 (v/v) (0.5 mg mL^{-1}) with stirring at 60 °C for 1 h. PCBM was dissolved in CB (20 mg mL^{-1}) and stirred at 60 °C for 1 h. HDPA was dissolved in EtOH (0.3 mg mL^{-1}).

2.3. Solar Cell Fabrication. Prepatterned indium tin oxide (ITO) (active areas of 0.09 and 0.16 cm^2) glass substrates (Naranjo, 15 Ω sq^{-1}) were sequentially cleaned by sonication in acetone for 15 min, scrubbing and 15 min of sonication in an aqueous sodium dodecyl sulfate solution, rinsing with deionized water for 15 min, and sonication in 2-propanol for 15 min. After drying the substrates with a N_2 gun, they were treated with ultraviolet (UV)—ozone for 30 min, before being transferring to a N_2-filled glovebox.

First, 120 μL of NiO_x was spin coated at 3000 rpm with 1000 s^{-1} acceleration for 30 s. Then, 120 μL of Me-4PACz solution was spin coated at 3000 rpm with 1000 rpm s^{-1} acceleration for 30 s, after which these layers were annealed together for 10 min at 100 °C. After cooling down to room temperature, 120 μL of Al_2O_3 dispersion was spin coated at 4000 rpm with 2000 rpm s^{-1} acceleration for 30 s and annealed at 100 °C for 5 min. For the perovskite, 120 μL of precursor solution was spin coated at 4000 rpm with 1000 rpm s^{-1} acceleration for 32 s, and 150 μL anisole was dropped after 28 s from the start of spinning. The perovskite layer was then annealed for 15 min at 100 °C. After cooling to room temperature, 120 μL of $PDAI_2$ solution was dynamically spin coated at 4000 rpm for 30 s and annealed at 100 °C for 5 min. Then, 120 μL of PCBM solution was spin coated at 1000 rpm with 1000 rpm s^{-1} acceleration for 30 s, without further annealing. The samples were then transferred to a thermal evaporator, where 8 nm of BCP and 100 nm of Ag were deposited under high vacuum (<10^{-7} Torr).

https://doi.org/10.1021/acsaem.5c02216
ACS Appl. Energy Mater. 2025, 8, 14486−14497

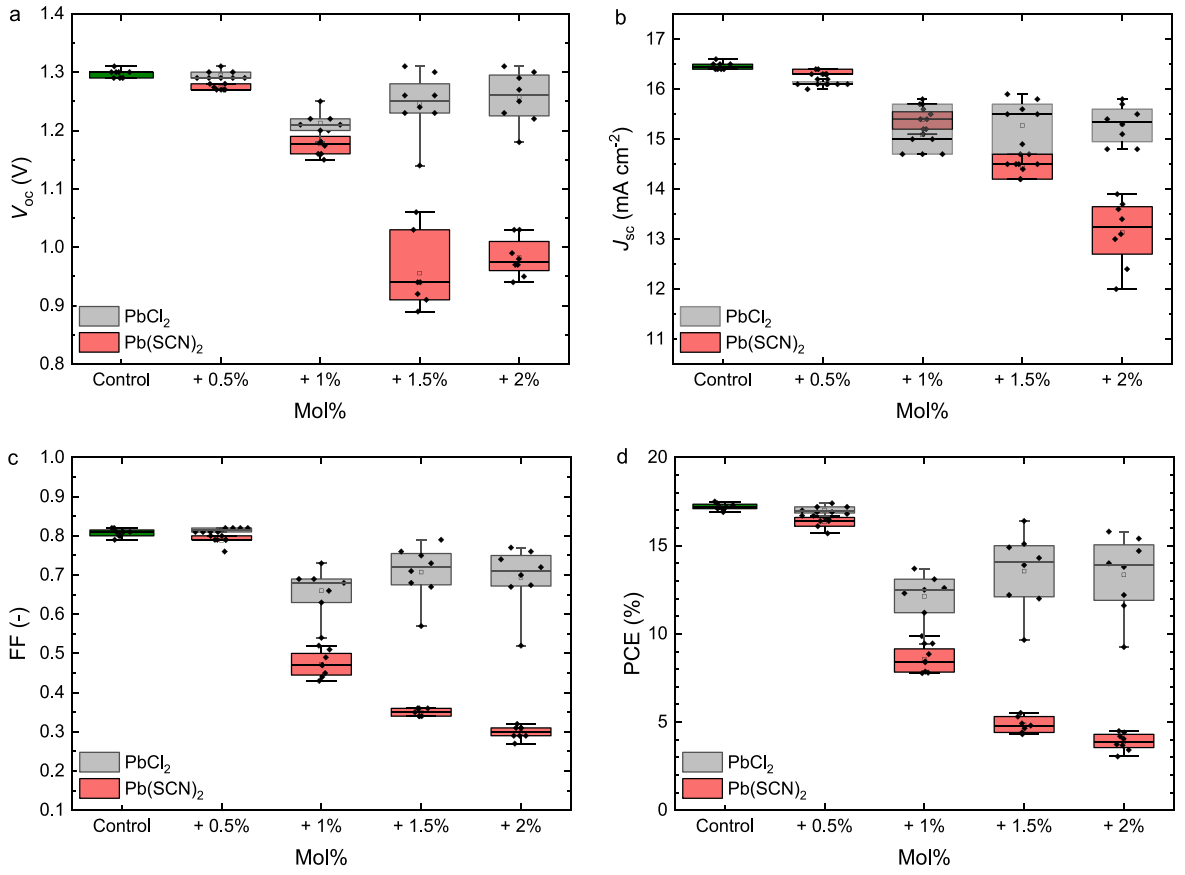

Figure 1. Boxplots of the photovoltaic parameters (a) V_{oc}, (b) J_{sc}, (c) FF, and (d) PCE, of ITO|NiO_x|Me-4PACz|Al_2O_3|$Cs_{0.2}FA_{0.8}Pb(I_{0.6}Br_{0.4})_3$|$PDAI_2$|PCBM|BCP|Ag solar cells processed without and with different mol % of $Pb(SCN)_2$ or $PbCl_2$ as additive to the precursor solution. The boxplots show the mean (open square), median (center line), 25th and 75th percentiles (box limits), and minimum and maximum (whiskers).

2.4. Film Characterization. Scanning electron microscopy (SEM) images were collected with a FEI Quanta 3D FEG microscope (5 keV electron beam, secondary electron detector) and a PhenomProX (5 keV electron beam, secondary electron detector). X-ray diffraction (XRD) was recorded with a Bruker 2D phaser (Cu Kα radiation, λ = 1.5406 Å). Measurements were performed in the range of 10−40° with a step size of 0.05° and a collection time of 0.5 s. A divergence slit of 0.6 mm and an antiscatter screen of 0.5 mm were used. X-ray photoelectron spectroscopy (XPS) measurements were performed using a Thermo-Scientific K-Alpha with a 180° double-focusing hemispherical analyzer and a 128-channel detector. Monochromatic Al Kα (1486.6 eV) radiation was used, and the X-ray spot size was 400 μm. The depth-profile measurements were performed in etching mode with an ion energy of 500 eV and low current (sputter rate estimate of 0.05 nm s^{-1}). Each etch cycle had a duration of 30 s and 90 total levels were measured.

2.5. Device Characterization. Solar cells were tested in a N_2-filled glovebox at ambient temperature. To emulate approximately 100 mW cm^{-2} AM1.5G light, a tungsten halogen lamp in combination with a Schott GG385 UV filter, and Hoya LB120 daylight filter were used. Incident light was referenced using a Si photodiode. Shadow masks of 0.0676 or 0.1296 cm^2 were used to define the illuminated area of the solar cell. Current density—voltage (J–V) characteristics were determined using a Keithley 2400 SMU. The J–V scan swept the applied voltage bias (without prebiasing) from +1.5 to −0.1 V for a reverse scan, or from −0.1 to +1.5 V for a forward scan using a scan rate of 250 mV s^{-1} with 161 steps. For regular external quantum efficiency (EQE) measurements, a tungsten halogen lamp (Philips Focusline, 50 W) was used and its light was mechanically chopped at 165 Hz (Stanford Research SR540) before passing through a monochromator (Oriel Cornerstone 130) and an aperture (0.0314 cm^2). The cell response was measured using a low-noise current preamplifier (Stanford Research SR570) in combination with a lock-in amplifier (Stanford Research SR830). The incident light intensity was referenced using a Si detector. 1-Sun light bias was simulated using a 530 nm LED (Thorlabs M530L3) driven by a Thorlabs DC4104 driver to accurately determine short-circuit current density (J_{sc}) under approximately AM1.5G conditions. Highly sensitive EQE measurements used the light from an Osram 64655 HLX 250 W tungsten halogen lamp mechanically chopped at 333 Hz passing appropriate sorting filters and dispersed using an Oriel Cornerstone 260 monochromator. The response was recorded using a Stanford Research SR570 preamplifier and a Stanford Research SR830 lock-in amplifier. Calibration was performed using reference Si and InGaAs detectors. The measured highly sensitive EQE spectra were scaled to regular EQE data.

2.6. Quasi-Fermi Level Splitting. The quasi-fermi level splitting (QFLS) was assessed through steady-state absolute photoluminescence (ss-PL) measurements. Samples were excited using a 455 nm Thorlabs M455F3 fiber-coupled LED. Samples were placed under an Avantes AvaSphere-30-REFL integrating sphere equipped with in-line filter holders for excitation light and emitted light, holding a 550 nm short-pass filter (Edmund Optics) and a 550 nm long-pass filter (Edmund Optics), respectively. The incident photon flux was adjusted to simulate AM1.5G conditions. The integrating sphere was connected to an Avantes AvaSpec-HSC1024 × 58TEC-EVO spectrometer (550−1100 nm) by an optical fiber. The setup was calibrated using an Avantes halogen lamp, yielding a spectral correction factor. Spectral photon fluxes ϕ_{PL} were obtained after a Jacobian transformation. Using the nonlinear least-squares fit method in MATLAB, the QFLS (ΔE_F) was determined from the ϕ_{PL}. The relation between QFLS and photon flux is defined as follows

https://doi.org/10.1021/acsaem.5c02216
ACS Appl. Energy Mater. 2025, 8, 14486−14497

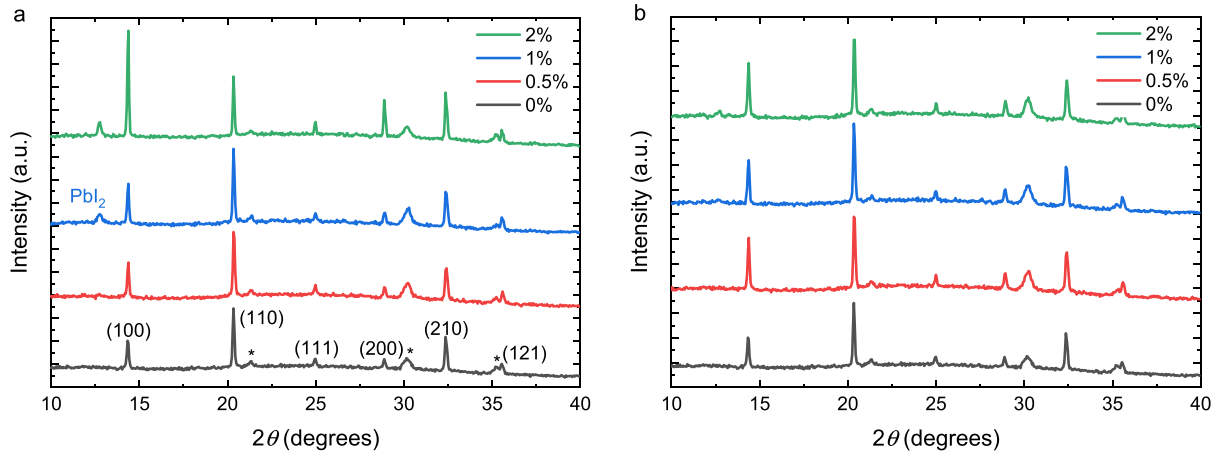

Figure 2. X-ray diffractograms of stoichiometric $Cs_{0.2}FA_{0.8}Pb(I_{0.6}Br_{0.4})_3$ perovskite films (0 mol %) and films processed with 0.5, 1, and 2 mol % of additive. (a) $Pb(SCN)_2$. (b) $PbCl_2$. Peaks were assigned by assuming a cubic unit cell in the space group $Pm\bar{3}m$. Peaks indicated with an asterisk are from ITO.

$$\phi_{PL}(E) = \frac{1}{4\pi^2 h^3 c^2} \frac{a(E)E^2}{\exp\left(\frac{E-\Delta E_F}{k_b T}\right) - 1}$$

where $a(E)$ is the photon energy-dependent absorptivity, which is assumed to be unity for photon energies sufficiently larger than the optical bandgap. Each film or (partial) stack combination was measured on 3 spots on the same film and on multiple films, the QFLS values were averaged and the standard deviation was determined. Next to variations in QFLS for different spots on the sample, there are batch-to-batch variations to inevitable small differences in the composition of the precursor solutions and processing conditions during the investigations. From the available data the standard deviation between nominally identical samples is estimated to be 15 meV or less.

3. RESULTS AND DISCUSSION

3.1. Lead Thiocyanate and Lead Chloride Additives.

To study the effect of lead-salt additives, we fabricate inverted ($p-i-n$) ITO|NiO_x|Me-4PACz|Al_2O_3|$Cs_{0.2}FA_{0.8}Pb(I_{0.6}Br_{0.4})_3$|$PDAI_2$|PCBM|BCP|Ag solar cells. The $Cs_{0.2}FA_{0.8}Pb(I_{0.6}Br_{0.4})_3$ perovskite layer is processed from a single precursor solution, using anisole as antisolvent, and thermal annealing to create a polycrystalline perovskite thin film. In optimized devices, this wide-bandgap perovskite (1.77 eV) provides a V_{oc} of 1.30 V, a J_{sc} of 16.5 mA cm^{-2}, a fill factor (FF) of 0.82, and a PCE of 17.5% (Figure S1). Adding $Pb(SCN)_2$ into the precursor solution in molar ratios in the range of 0.5−2 mol % with respect to lead, results in a decrease of all photovoltaic parameters (Figures 1 and S1). We attribute this loss in performance primarily to a disturbance of the perovskite stoichiometry. It is widely reported that SCN^- anions volatize during thermal annealing of the perovskite layer, according to the following reactions[19]

$$2(NH_2)_2CHI + Pb(SCN)_2 \rightarrow PbI_2 + 2(NH_2)_2CHSCN \quad (1)$$

$$(NH_2)_2CHSCN \rightarrow NH_2CHNH \uparrow + HSCN\uparrow \quad (2)$$

These reactions imply that the addition of $Pb(SCN)_2$ results in the formation of PbI_2 and a deficiency of FAI, because a proton of FAI is consumed to form the volatile thiocyanic acid (HSCN), which leads to the concomitant loss of formamidine (NH_2CHNH). The formation of PbI_2 is evidenced by the appearance of the characteristic (001) reflection at 12.7° in the XRD (Figure 2a) and by the formation of PbI_2 crystallites on the perovskite surface in the SEM images (Figure S2). We note that the intensities of the Bragg peaks varied somewhat between nominally identical samples and should not be interpreted quantitatively; they rather serve as a qualitative description of the structural composition of the films. XPS surface scans of films processed with 5 mol % of $Pb(SCN)_2$ (Figure S3) confirm the formation of excess PbI_2 by the increased intensity of the I 3d and Pb 4f photoelectron peaks, implying higher I^- and Pb^{2+} contents, and a I^-/Pb^{2+} ratio closer to 2 (2.73 without additive, and 2.61 with additive) at the top surface of films processed with 5 mol % $Pb(SCN)_2$.

These results demonstrate that the annealed $Cs_{0.2}FA_{0.8}Pb(I_{0.6}Br_{0.4})_3$ films do not have the overall perfect ABX_3 stoichiometry when processed with $Pb(SCN)_2$ as an additive, but rather exist in a form with deficiencies of the A-site (FA^+, Cs^+) and X-site (I^-, Br^-) ions and thus an excess of B-site (Pb^{2+}) cations. Tauc plots reveal that increasing the concentration of the $Pb(SCN)_2$ additive widens the bandgap by up to approximately 7 meV at 2 mol % (Figure S4). Qualitatively, the wider bandgap is explained by the evaporation of formamidine from the $Cs_{0.2}FA_{0.8}Pb(I_{0.6}Br_{0.4})_3$ perovskite film which increases the Cs^+/FA^+ ratio, and by the formation of PbI_2, which increases the Br^-/I^- ratio within the perovskite phase. Assuming that reactions (1) and (2) occur to the full extent, the addition of α mole of $Pb(SCN)_2$ per mole of lead results in a change of perovskite composition given by

$$0.4PbI_2 + 0.6PbBr_2 + 0.8FAI + 0.2CsI + \alpha Pb(SCN)_2 \rightarrow 2\alpha FASCN(\uparrow) + 3\alpha PbI_2 + (1-2\alpha)Cs_{0.2/(1-2\alpha)} FA_{(0.8-2\alpha)/(1-2\alpha)}Pb[I_{(0.6-2\alpha)/(1-2\alpha)}Br_{0.4/(1-2\alpha)}]_3 \quad (3)$$

Hence, at $\alpha = 0.02$ (2 mol % of additive) the Cs^+/FA^+ ratio $[1/(4-10\alpha)]$ changes from the original 0.250 to 0.263 and the Br^-/I^- ratio $[1/(1.5-5\alpha)]$ from 0.667 to 0.714. The slightly higher Cs^+/FA^+ ratio would give a rise in bandgap of about 1.5 meV,[26] whereas the expected increase in bandgap as a consequence of the higher Br^-/I^- is approximately 10 meV, based on experiments where we varied the Br^- content of the above-mentioned composition between 0 and 40%. The total expected blue shift of approximately 11.5 meV is larger than the 7 meV shift observed experimentally and indicates a lower

https://doi.org/10.1021/acsaem.5c02216
ACS Appl. Energy Mater. 2025, 8, 14486−14497

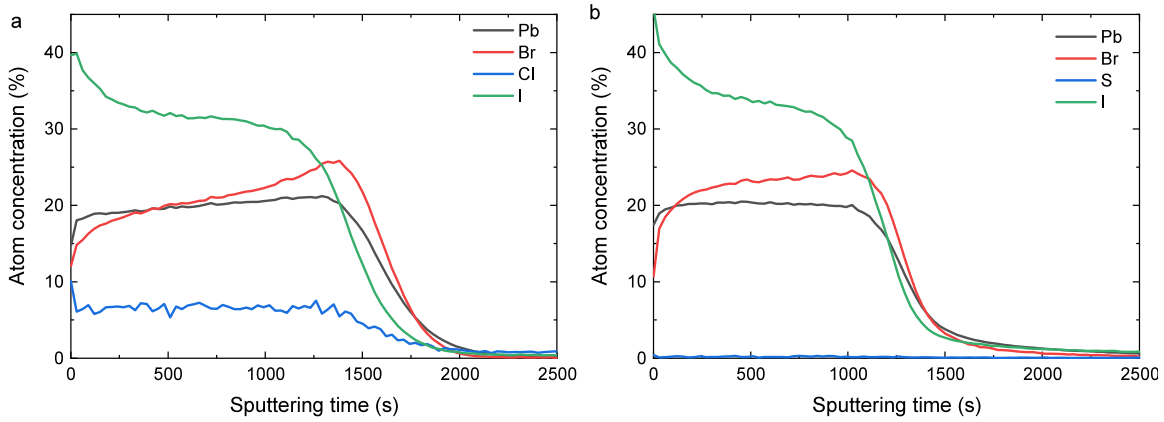

Figure 3. XPS-depth profiles of a perovskite alloyed with (a) 5 mol % $PbCl_2$ and (b) 5 mol % of $Pb(SCN)_2$. More detailed information regarding the elemental distribution is shown in Figure S6.

Br^-/I^- ratio than 0.714, which can occur when not all 3α PbI_2 is expelled from the perovskite lattice. This would create a deficiency of A- and X-side ions and a nonstoichiometric perovskite.

The minor A- and X-site ion deficiencies that result from processing with 0.5 mol % of $Pb(SCN)_2$ as additive, reduce device performance only marginally but all parameters are significantly affected at concentrations of 1 mol % or higher (Figure 1). This presumably stems from the significant increase of PbI_2 at the top surface of the perovskite, which is reported to facilitate charge recombination and thus reduce the V_{oc},[27] while simultaneously hampering charge extraction due to its insulating nature.[28]

When $PbCl_2$ is used as an additive, the $Cs_{0.2}FA_{0.8}Pb(I_{0.6}Br_{0.4})_3$ solar cells show a much smaller drop in performance (Figure 1). A small amount (0.5 mol %) of $PbCl_2$ even slightly improves the V_{oc} by 10 mV, in agreement with previous studies where $PbCl_2$ was found to facilitate the incorporation of Cl^- into the perovskite lattice, resulting in the passivation of trap states and an increased charge mobility, which both reduce charge recombination losses.[29] However, the small increase in V_{oc} might also stem from the slight increase in bandgap due to the substitution of iodine with chloride. For this concentration, the slight increase in V_{oc} is accompanied by a change in the XRD pattern (Figure 2b) where the intensity of the (100) diffraction peak at 14.4° increases compared to the (200) peak at 28.8° without an observable shift of the (100) peak position. Further increasing the $PbCl_2$ concentration in the precursor solution leads to a reduction of J_{sc}, which is again ascribed to the formation of excess lead iodide at the surface that acts as an insulating layer, as shown in the SEM images (Figure S5).[28] It is evident that a deviation from the ideal stoichiometry is detrimental for device performance.

Depth profiling XPS (Figures 3 and S6) on films with 5 mol % of additive reveals that chlorine is present in the annealed perovskite films processed with $PbCl_2$, but that—in contrast—no sulfur is present when $Pb(SCN)_2$ was used. Apparently Cl^-, with its smaller ionic radius than Br^- or I^-, is easily built into the perovskite lattice but SCN^- is not. Although the radius of SCN^- (2.13 Å) has been reported to be in between that of Br^- (1.96 Å) and I^- (2.20 Å),[30] the length of approximately 3 Å of the linear SCN^- ion makes that it cannot be accommodated in the regular cubic perovskite crystal structure. Accordingly, $A_2Pb(SCN)_2X_2$ perovskites (with A = MA, FA, or Cs and X = Br or I) adopt a layered structure in which Pb^{2+} is octahedrally coordinated by four halide ions and by two S-bonded thiocyanate ligands in a trans position with their N-termini directed to the interlayer space.[31−34] Thus, the favorable Pb−S bonding compared to Pb−N bonding, causes that $Pb(SCN)_2X_4$ octahedra are linked into layers through corner-sharing halide ligands, while the thiocyanate ligands disconnect the octahedral network. Incorporation of thiocyanate into a $FAPbI_3$ perovskite to form $FA_6Pb_4I_{13\cdot5}(SCN)_{0.5}$ and $FA_4Pb_2I_{7\cdot5}(SCN)_{0.5}$ phases has been shown to result in columnar defects.[35,36] When using $Pb(SCN)_2$ as an additive in small molar excess, such columnar defects are likely to form at grain boundaries and emerge at the crystallite surfaces.

When $PbCl_2$ is converted into perovskite, it consumes one equivalent of FAI to maintain stoichiometry, according to

$$PbCl_2 + (NH_2)_2CHI \rightarrow [(NH_2)_2CH]Pb(Cl_{0.66}I_{0.33})_3 \quad (4)$$

and assuming that α mole $PbCl_2$ as additive is incorporated into the perovskite, this would leave α mole of PbI_2 unreacted, according to

$$0.4PbI_2 + 0.6PbBr_2 + 0.8FAI + 0.2CsI + \alpha PbCl_2 \rightarrow \alpha PbI_2 + Cs_{0.2}FA_{0.8}Pb[I_{(0.6-2\alpha)/3}Br_{0.4}Cl_{2\alpha/3}]_3 \quad (5)$$

In contrast to the perovskite films deposited with $Pb(SCN)_2$, the use of $PbCl_2$ does not change the initial Cs^+/FA^+ ratio of 0.25. When 2 mol % (α = 0.02) of $PbCl_2$ is used as additive, the Br^-/I^- ratio $[1/(1.5-5\alpha/3)]$ changes from 0.667 to 0.682, which is expected to blue-shift the bandgap by approximately 3 meV. Additionally, the Cl^-/I^- ratio $[2\alpha/(1.8-2\alpha)]$ changes from 0 to 0.023, resulting in an estimated blue-shift of the bandgap by approximately 11 meV.[37] Again, the total expected shift of 14 meV is somewhat larger than the experimental value of approximately 7 meV (Figure S7).

As noted, the observed bandgap shifts of 7 meV when using 2 mol % $Pb(SCN)_2$ or $PbCl_2$ are slightly smaller than the shifts of 11.5 and 14 meV, predicted when assuming that reactions (3) and (5) occur to the full extent. The uncertainty of the experiment and the predictions is several meV, which may explain this difference in part. It is also possible that the lead halide expelled in reactions (3) and (5) is not exclusively PbI_2, but also contains $PbBr_2$ or $PbCl_2$. In such case the resulting Br^-/I^- ratio is closer to the original value of 0.667. This would reduce the difference between the expected and experimentally obtained shifts. However, XPS depth profiling (Figures 3a and

https://doi.org/10.1021/acsaem.5c02216
ACS Appl. Energy Mater. 2025, 8, 14486−14497

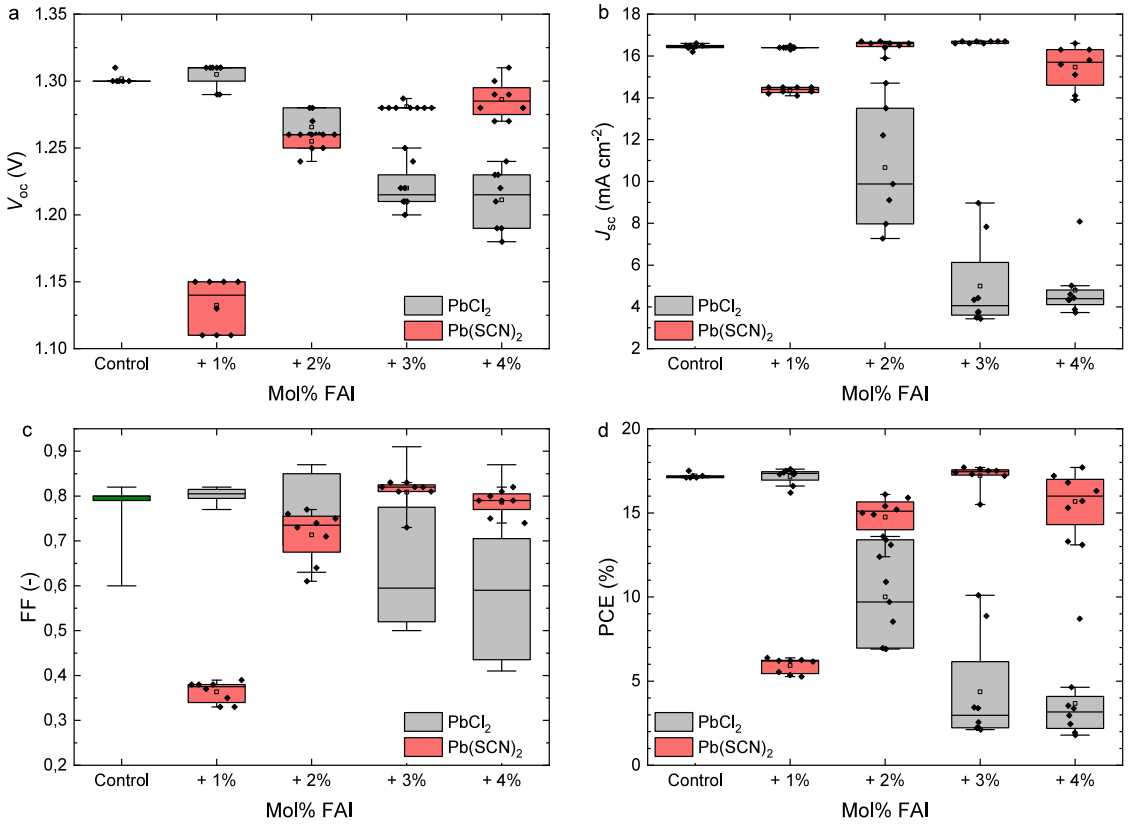

Figure 4. Boxplots of the photovoltaic parameters (a) V_{oc}, (b) J_{sc}, (c) FF, and (d) PCE, of ITO|NiO$_x$|Me-4PACz|Al$_2$O$_3$|Cs$_{0.2}$FA$_{0.8}$Pb(I$_{0.6}$Br$_{0.4}$)$_3$|PDAI$_2$|PCBM|BCP|Ag solar cells (8 devices per variation, measured as reverse scan) processed without and with 1 mol % Pb(SCN)$_2$ or PbCl$_2$ as additive to the precursor solution together with 1−4 mol % excess FAI. The boxplots show the mean (open square), median (center line), 25th and 75th percentiles (box limits), and minimum and maximum (whiskers).

S6) suggests an increased concentration of iodide, and possibly chloride, at the surface, suggesting that mainly PbI$_2$ is formed. We have found no evidence for the formation of other phases from XRD. In case quasi-2D domains would form,[35,36] these would have a much wider bandgap.

3.2. Compensating for the Loss of Stoichiometry.

Following reaction (4), the addition of PbCl$_2$ consumes one equivalent of FAI when it is converted into perovskite and leaves one equivalent of lead halide unreacted. In contrast, the combination of reactions (1) and (2) shows that addition of Pb(SCN)$_2$ creates a 3-fold deficiency in FAI: two FAI equivalents are necessary to compensate for the evaporation of two formamidine molecules and one FAI to convert the PbI$_2$ that is formed in reaction (1) into a perovskite. To confirm that disturbing the ABX$_3$ stoichiometry is the primary cause for degrading device performance, we employed either Pb(SCN)$_2$ or PbCl$_2$, together with additional FAI to restore the ABX$_3$ stoichiometry by supplying additional A-site and X-site ions to react with the excess Pb^{2+} stemming from the lead-salt additives. Following this concept, the equivalents of FAI required to restore the stoichiometry and device performance should be related to the fraction of the lead-salt additive that is built into the perovskite lattice. This implies that, according to reaction (4), adding PbCl$_2$ to the perovskite precursor requires one additional equivalent of FAI to be added to ensure full conversion of the additives to a stoichiometric photoactive phase. On the other hand, the absence of SCN$^-$ in the perovskite indicates that Pb(SCN)$_2$ merely provides excess Pb^{2+} to the annealed additive-rich film, while consuming the available FAI to form formamidine and thiocyanic acid, according to reactions (1) and (2). Accordingly, three additional equivalents of FAI are required per equivalent of Pb(SCN)$_2$ added to achieve full conversion of the additive into a stoichiometric photoactive perovskite phase, according to

$$3(NH_2)_2CHI + Pb(SCN)_2 \rightarrow [(NH_2)_2CH]PbI_3 + 2(NH_2)_2CHSCN(\uparrow) \quad (6)$$

there with effectively adding [(NH$_2$)$_2$CH]PbI$_3$ to the perovskite composition.

To test our hypothesis, we added 1 mol % of PbCl$_2$ or Pb(SCN)$_2$ into the perovskite precursor solution, along with 1−4 mol % of excess FAI. As illustrated in Figure 4, the photovoltaic parameters show that employing 1 mol % of PbCl$_2$ or Pb(SCN)$_2$ as additive restores device performance when the addition is compensated by a specific additional amount of FAI, which is one equivalent of FAI for PbCl$_2$ and three equivalents of FAI for Pb(SCN)$_2$. Adding α mole of PbCl$_2$ and α mole of FAI per mole of lead to the precursor solution leads to a perovskite composition given by

$$0.4PbI_2 + 0.6PbBr_2 + (0.8+\alpha)FAI + 0.2CsI + \alpha PbCl_2 \rightarrow (1+\alpha)Cs_{0.2/(1+\alpha)}FA_{(0.8+\alpha)/(1+\alpha)}Pb[I_{(0.6+0.33\alpha)/(1+\alpha)}Br_{0.4/(1+\alpha)}Cl_{0.66\alpha/(1+\alpha)}]_3 \quad (7)$$

whereas adding α mole of Pb(SCN)$_2$ and 3α mole of FAI per mole of lead to the precursor leads to

https://doi.org/10.1021/acsaem.5c02216
ACS Appl. Energy Mater. 2025, 8, 14486−14497

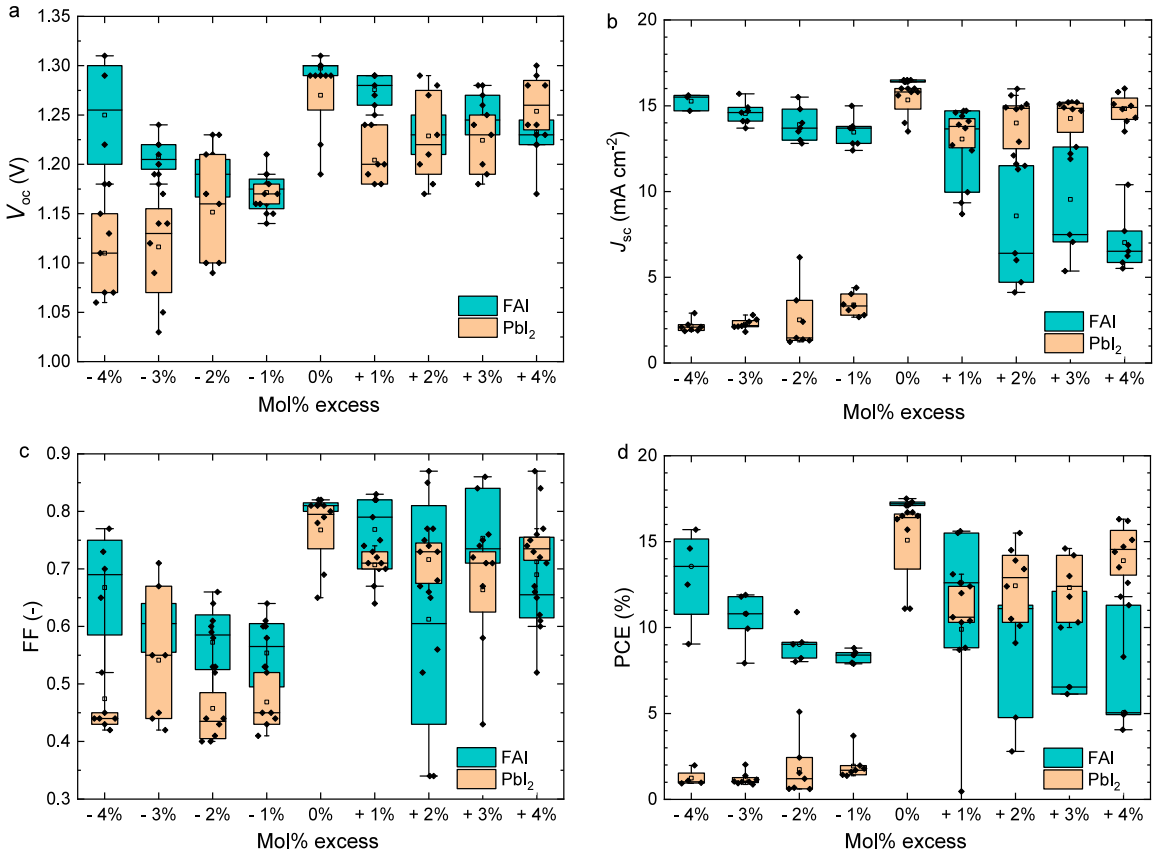

Figure 5. Boxplots of the photovoltaic parameters (a) V_{oc}, (b) J_{sc}, (c) FF, and (d) PCE, of ITO|NiO_x|Me-4PACz|Al_2O_3|$Cs_{0.2}FA_{0.8}Pb(I_{0.6}Br_{0.4})_3$|$PDAI_2$|PCBM|BCP|Ag solar cells (8 devices per variation, measured as reverse scan) processed with −4 to +4 mol % of either PbI_2 or FAI in the precursor solution. The boxplots show the mean (open square), median (center line), 25th and 75th percentiles (box limits), and minimum and maximum (whiskers). 0% mol excess represents fully stoichiometric films.

$$0.4PbI_2 + 0.6PbBr_2 + (0.8 + 3\alpha)FAI + 0.2CsI + \alpha Pb(SCN)_2 \rightarrow 2\alpha FASCN(\uparrow) + (1 + \alpha)Cs_{0.2/(1+\alpha)}FA_{(0.8+\alpha)/(1+\alpha)}Pb[I_{(0.6+\alpha)/(1+\alpha)}Br_{0.4/(1+\alpha)}]_3 \quad (8)$$

The difference between $PbCl_2$ and $Pb(SCN)_2$ supports the idea that Cl^- does not volatize as HCl during thermal annealing. In that case, the overall stoichiometry would not be maintained in the annealed film with a 1:1 molar ratio of $PbCl_2$:FAI, and one equivalent of FAI would still result in an X-site anion deficiency. However, Figure 4 shows that exceeding the required 1:1 ratio of FAI: $PbCl_2$ is detrimental to device performance, especially regarding the J_{sc}. This observation is already widely reported in the literature and stems from the accumulation of excessive organic cations due to ion migration at the interface that severely hampers charge extraction, since this inevitably leads to energy level misalignment and increased recombination losses.[38] This is also recognized by the significant increase in hysteresis when adding additives in increasing amounts (Figure S8a). X-ray diffractograms (Figure S9b) reveal the presence of a small amount of PbI_2 in the reference sample and in the sample with (1 mol % $PbCl_2$ + 1 mol % FAI), which is supported by SEM images (Figure S10) that show white crystallites on top of the perovskite surface. No PbI_2 is found once the FAI excess exceeds 1 mol %, confirming that excess FAI binds to excess PbI_2 that would otherwise reside on the perovskite surface. Increasing the FAI excess beyond 1 mol % increases the (100)/(110) peak ratio, but also leads to the formation of pinholes as shown in Figure S10, possibly due to the larger excess of volatile FAI. Finally, Tauc plots (Figure S11d) show a blue-shift of the bandgap with 1 mol % of $PbCl_2$, as was shown previously. Simultaneous addition of 1 or 2 mol % of excess FAI shifts the bandgap toward that of the reference, whereas a significant red-shift of the bandgap is observed when adding more excess FAI (3 4 mol %). This suggests that 1 mol % of FAI leads to a stoichiometric perovskite when 1 mol % of $PbCl_2$ is used as additive.

For $Pb(SCN)_2$, a FAI deficiency severely affects both the V_{oc} and FF, while the J_{sc} remains somewhat unaffected, as shown in Figure 4. The large drop in voltage and FF is expected due to the presence of halide vacancies stemming from the FAI deficiency, as well as the unformed PbI_6^{4-} octahedra due to a deficiency of both A- and X-site ions. The ideal 1:3 ratio of $Pb(SCN)_2$:FAI supports our assumption that SCN^- is fully volatized during annealing and is not built into the lattice. Hence, according to reaction (4), the consumed FAI must be compensated for, while the excessively formed PbI_2 requires additional FAI to be converted into the photoactive $FAPbI_3$ phase. This reaction mechanism is further verified by X-ray diffractograms (Figure S9a), where a FAI excess below 2 mol % leads to a significant trace of residual PbI_2. SEM images (Figure S10) further verify that 3 mol % of excess FAI is required to eliminate undesirable PbI_2 crystals on the perovskite surface. Similarly to using $PbCl_2$, providing more FAI than required to compensate for the disturbed

https://doi.org/10.1021/acsaem.5c02216
ACS Appl. Energy Mater. 2025, 8, 14486−14497

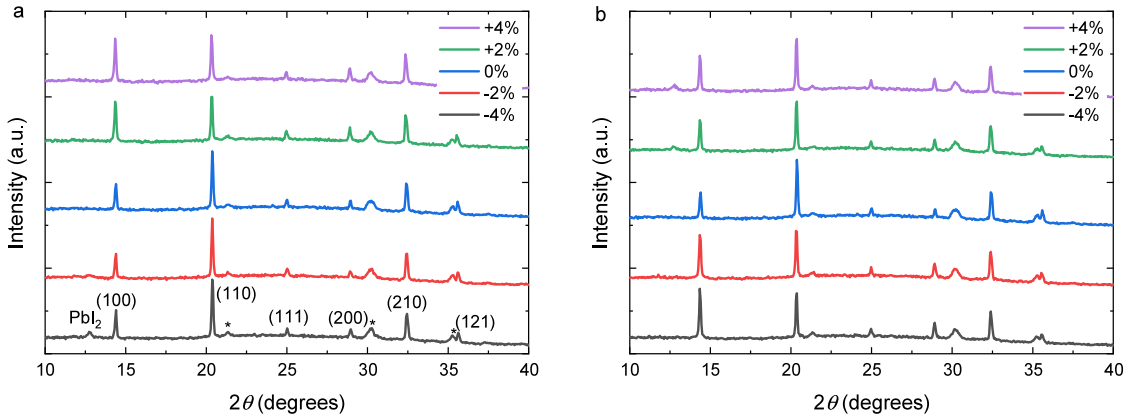

Figure 6. X-ray diffractograms of $Cs_{0.2}FA_{0.8}Pb(I_{0.6}Br_{0.4})_3$ perovskite films prepared from precursor solutions with different mole percent excess or deficiency of either FAI (a) or PbI_2 (b). Peaks were assigned by assuming a cubic unit cell in the space group $Pm\bar{3}m$. Peaks indicated with an asterisk are from ITO.

stoichiometry increases the (100)/(110) peak ratio, but has negative effects on device performance due to a combination of pinholes and the presence of excessive organic cations. Tauc plots (Figure S11c) show a blue-shift of the bandgap when using $Pb(SCN)_2$ and reveal only minor shifts for FAI excesses below 3 mol %. Adding 3 mol % of excess FAI red-shifts the bandgap slightly beyond that of the reference, but a significant red-shift is observed at 4 mol % which exceeds the FAI excess that is required to restore the stoichiometry. This illustrates that beyond the optimal FAI excess, the iodide/bromide ratio within the absorber is affected.

Both the depth-profile XPS (Figure 3) and the blue-shift of the bandgap with increasing $PbCl_2$ concentration (Figure S7) support that Cl^- is built into the lattice while SCN^- is not. The results shown in Figure 4 demonstrate that adding additional FAI in the correct amount can compensate for the offset ABX_3 stoichiometry caused by the lead-salt additives. The different behavior of Cl^- and SCN^- likely originates from two complementary effects. First, as argued above, Cl^- is built easier into the 3D perovskite lattice than SCN^- due to their atomic radii. Second, the fact that Cl^- is a weaker base than SCN^- favors the loss of HSCN ($pK_a \approx -1$) over that of HCl ($pK_a \approx -6$) during thermal annealing.

3.3. Perturbing the Precursor Stoichiometry. Having illustrated that maintaining stoichiometry is essential to achieve proper device performance when using lead-salt additives, we delve deeper into the stoichiometry of an additive-free perovskite by deliberately unbalancing the stoichiometry of the optimized precursor solution through solely changing the FAI or PbI_2 content. Thereby, we intentionally cause an excess or deficiency of either FAI or PbI_2 within the precursor solution. Figure 5 summarizes the effect on the solar cell performance parameters by deliberately offsetting the stoichiometry by withholding or adding up to 4 mol % of either PbI_2 or FAI into the precursor solution. The changes in J_{sc} for these off-stoichiometry devices seen in Figure 5b are confirmed by the changes in external quantum efficiency (EQE) spectra (Figures S12 and S13).

Figure 5 reveals that devices made from stoichiometric precursor solutions perform the best and that any deviation from the ideal stoichiometry is detrimental for device performance. Figure 5b shows that a PbI_2 deficiency leads to a nearly complete loss of photocurrent, which could stem from unformed PbI_6^{4-} octahedra due to the lack of sufficient Pb^{2+}, resulting in an excessive amount of defects that in turn act as charge traps. Likewise, an excess of FAI rapidly reduces the PCE, also mainly by a loss of J_{sc}, which is likely caused by the accumulation of organic cations near the interface with the electron transport layer (ETL) that impede charge extraction.

On the other hand, a FAI deficiency severely affects the FF and V_{oc} due to the presence of both halide vacancies and the deficiency of FA^+. Surprisingly, the impact of the FAI deficiency and PbI_2 excess on the PCE lessens when further increasing the offset from the optimum stoichiometry. One speculation for this is that a slight FAI deficiency or PbI_2 excess does not yet result in the formation of a PbI_2 phase, but is rather accommodated by creating FA^+ and I^- vacancies in the photoactive perovskite phase. When the FAI deficiency, and thus PbI_2 excess, becomes sufficiently large, it may form a separate PbI_2 phase, which then reduces the defect concentration in the perovskite phase. The XRD patterns of the films (Figure 6a) show signatures of PbI_2 at the highest FAI deficiency. However, it must be noted that aside from the increasing PCE with larger stoichiometric offsets of the FAI deficiency or the PbI_2 excess, this simultaneously leads to severe hysteresis (Figure S8b), likely stemming from increased ionic movements and rendering these layers unsuitable for solar cells.

Figure 6 shows that the changes in the X-ray diffractograms of perovskite films with excess PbI_2 are similar to those with a deficiency of FAI. With increasing FAI deficiency or PbI_2 excess, a diffraction peak appears at 12.7°, indicating the formation of PbI_2, as also observed in the SEM images (Figure S14). Furthermore, the SEM images (Figure S14) verify that increasing the PbI_2 excess beyond stoichiometric concentration leads to direct expulsion of excess PbI_2 crystallites toward the perovskite film surface, which obeys a similar mechanism as a deficiency of FAI. On the other hand, an excess of FAI or deficiency of PbI_2 leads to a significant increase in the number of pinholes in the film and an increasing (100) peak intensity (Figure 6), which is likely related to the increasing excess of FA^+ that has to be expelled from the film during crystallization of the perovskite layer.

To investigate what happens with these stoichiometric offsets during film fabrication, we measured the absolute photoluminescence (APL) and extracted the QFLS for films with an excess or deficiency of either FAI or PbI_2. The APL was measured for $Cs_{0.2}FA_{0.8}Pb(I_{0.6}Br_{0.4})_3$ perovskites deposited

https://doi.org/10.1021/acsaem.5c02216
ACS Appl. Energy Mater. 2025, 8, 14486−14497

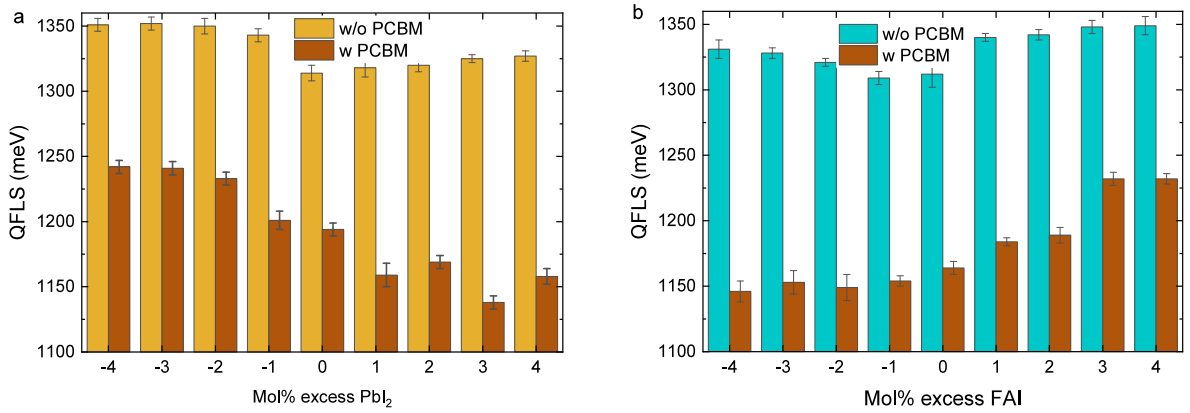

Figure 7. QFLS of $Cs_{0.2}FA_{0.8}Pb(I_{0.6}Br_{0.4})_3$ perovskite films processed from precursor solutions with films with excess or deficiency of PbI_2 (a) or FAI (b) without and with a PCBM layer on top.

on glass/ITO substrates functionalized with HDPA. Compared to other substrates and surface treatments, HDPA significantly improved reproducibility and resulted in consistent QFLS values.[39] Figure S15 shows that only small differences are found when films are measured from either glass or film sides. Surprisingly, any modification to the perovskite composition, albeit an excess or deficiency of either FAI or PbI_2, leads to a small increase in QFLS (Figure S15), but a PbI_2 deficiency or a FAI excess seem to have the most impact. Figure S16 shows the normalized PL spectra, which reveal minor variations in peak position (697 ± 3 nm) and peak width (fwhm 44.4 ± 0.8 nm), corresponding to small changes (approximately 15 meV) in bandgap. Even though the improvement of QFLS is small (<40 meV), it does not explain the rapid loss in device performance when the precursor solution deviates from the perfect stoichiometry (Figure 5). This finds its origin in the fact that the optically measured QFLS cannot always be directly correlated to device performance, because it is not sensitive to hindered charge extraction.[40] Stolterfoht et al. have shown that a mismatch between QFLS and V_{oc} is expected to occur when the diffusion of carriers to the metal contact or charge transport layer is slow compared to the nonradiative recombination in the interface region.[41] Rather, the QFLS provides information on the quality of the perovskite semiconductor and its interfaces with adjacent layers. Note that films with increasing excess of FAI or PbI_2 show opposite trends, in agreement with the argument that an excess of FAI leads to a deficiency of PbI_2 and vice versa. Indeed, the QFLS increases with PbI_2 deficiency or FAI excess, while a PbI_2 excess or FAI deficiency show minor impact. This suggests that a FAI excess is the main contributor to an increased QFLS. Possibly, the excess FAI migrates toward the top surface of the perovskite and passivates defect states at this interface which increases the QFLS, but at the same time hinders charge collection, resulting in sharp drops in J_{sc} and FF (Figure 5).

To verify our assumption and study how the losses at the ETL interface are affected by the absorber stoichiometry, we deposited PCBM on the same films and repeated the APL measurements (Figure 7). Consistent with previous studies,[42] application of a fullerene-based ETL leads to significant loss of QFLS as a consequence of nonradiative recombination at the perovskite-PCBM interface. The perovskite-PCBM interface is considered the limiting interface to the V_{oc}, where the degree of the loss is affected by absorber stoichiometry. Again, there is an opposite trend for FAI and PbI_2. Increasing the FAI excess reduces the interfacial losses, which is also found when increasing the PbI_2 deficiency. This observation is consistent with the assumption that excess FAI migrates toward the top surface and reduces interfacial losses between the perovskite and PCBM. The advantageous effect of a thin interlayer between the perovskite and fullerene on the QFLS was shown before for choline chloride and LiF.[40,42]

Given the increase in QFLS (Figure 7) and the simultaneous decline in device performance (Figure 5) with any stoichiometric offset, overpassivation—potentially caused by the combined presence of $PDAI_2$ and excess FAI or PbI_2 at the perovskite film surface—cannot be excluded. Therefore, we fabricated devices without interfacial passivation ($PDAI_2$), with an excess or deficiency of FAI of up to 4 mol % in the precursor solution, as shown in Figure S17. Once more, we clearly show that the precursor stoichiometry should be conserved to achieve optimal device performance. Any stoichiometric offset leads to a slight reduction of J_{sc} by up to 1.5 mA cm^{-2}, but its primary impact is on the voltage. With a slight FAI deficiency the V_{oc} increases by up to 30 mV, possibly due to the passivating properties of excess PbI_2 on the perovskite film surface (Figure S14). However, the insulating nature of PbI_2 and its detrimental effects on the FF and J_{sc} result in poor-performing devices. On the other hand, excess FAI leads to a significant loss of V_{oc} by approximately 300 mV, likely stemming from increase of perovskite film porosity (Figure S14) due to the volatile FAI or from a FAI-rich surface that hinders charge collection.

Highly sensitive sub-bandgap photocurrent spectra of devices with an excess and deficiency of FAI or PbI_2 (Figure S18) reveal the presence of two sub-bandgap contributions to the EQE at approximately 0.95 and 1.40 eV that are associated with defects at the perovskite-PCBM interface.[43] The small variations in peak position are a consequence of small variations in film thickness (420 ± 20 nm) that cause a change of interference of the sub-bandgap light in the layer stack. The exponential band tail allows to determine the Urbach energy (E_u), which is a measure of the energetic disorder in the absorber,[44] but can also be affected by interfacial defects in the region where the EQE becomes very small. Hence E_u is not predominantly sensitive to changes in the bulk or at interfaces. Figure 8 shows that E_u is affected by absorber stoichiometry. This is expected, because a disturbance of the ABX_3 stoichiometry inevitably results in an increased degree of energetic disorder, and therefore E_u increases with

https://doi.org/10.1021/acsaem.5c02216
ACS Appl. Energy Mater. 2025, 8, 14486−14497

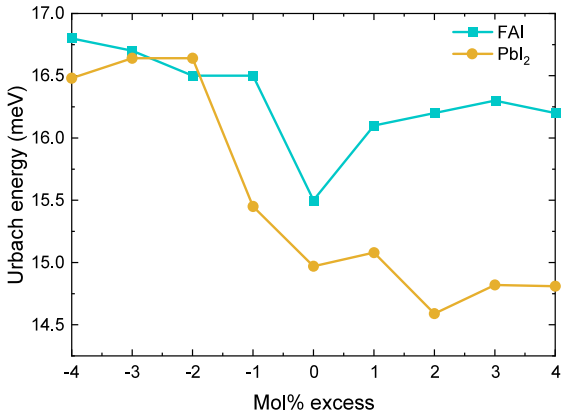

Figure 8. Urbach energies recorded from sub-bandgap EQE of ITO|NiO_x|Me-4PACz|Al_2O_3|$Cs_{0.2}FA_{0.8}Pb(I_{0.6}Br_{0.4})_3$|$PDAI_2$|PCBM|BCP|Ag solar cells processed from precursor solutions with stoichiometric compositions or with an excess or deficiency of PbI_2 or FAI.

increasing PbI_2 deficiency. A PbI_2 excess, however, has a small effect on the E_u. We propose that excess PbI_2 is not built into the crystal lattice and apparently has no significant effect on the E_u. When changing the FAI concentration, a low E_u is found for the stoichiometric composition as expected. For a FAI excess, the E_u is higher, similar to what is seen for a PbI_2 deficiency. For a FAI deficiency, the E_u does not decrease as seen for a PbI_2 excess.

4. CONCLUSIONS

The present study shows that it is essential to maintain the ABX_3 stoichiometry when producing perovskite solar cells. Using a wide-bandgap (1.77 eV) $Cs_{0.2}FA_{0.8}Pb(I_{0.6}Br_{0.4})_3$ perovskite, we find that adding low concentrations (0.5 to 2 mol %) of commonly used lead-salt additives ($PbCl_2$ and $Pb(SCN)_2$) to the precursor solution disturbs the stoichiometry of the perovskite absorber. The presence of excess Pb^{2+} leads to drastic reduction of device performance. This detrimental effect can be circumvented by simultaneously providing excess FAI to restore the stoichiometry to its original ABX_3 composition. Interestingly, the amount of FAI needed differs with lead-salt anion. Because Cl^- is incorporated into the crystal lattice and SCN^- is not, different amounts of FAI are required to restore the ABX_3 stoichiometry. For $PbCl_2$, adding one equivalent of FAI leads to the formation of stoichiometric $FAPb(Cl_{0.66}I_{0.33})_3$ and reinstates the optimized device performance, whereas $Pb(SCN)_2$ requires three equivalents of FAI to compensate the formation of excess PbI_2, which has to be converted into a $FAPbI_3$ stoichiometry and replace the formamidine that is lost during thermal annealing along with thiocyanic acid. While this study mainly focuses on lead-based additives, the stoichiometry-driven mechanism, by which additives affect the perovskite absorber composition, will likely also apply to lead-free additives (such as, e.g., NH_4Cl, NH_4SCN, FACl) as demonstrated from the analogous effects observed when creating an excess or deficiency of FAI.

Disturbing the stoichiometry of a perovskite absorber by a deliberate excess or deficiency of either FAI or PbI_2 in the precursor solution results in similar behavior and a slight disturbance has significant consequences for device performance. A FAI excess leads to detrimental changes in performance as a PbI_2 deficiency and vice versa. When subsequently adding an ETL we showed that, from a disturbed stoichiometry, the excess FAI migrates toward the top surface of the perovskite and significantly reduces interfacial non-radiative recombination losses, but does not result in improved device performance because of ionic accumulation and impeded charge extraction.

This study serves as a foundation for further research on additives, by emphasizing the importance of maintaining stoichiometry within the absorber.

■ ASSOCIATED CONTENT

Supporting Information

The Supporting Information is available free of charge at https://pubs.acs.org/doi/10.1021/acsaem.5c02216.

Contains additional $J-V$ characteristics, SEM images, box plots with hysteresis index, QFLS data and XPS, UV/vis, PL, and EQE spectra (PDF)

■ AUTHOR INFORMATION

Corresponding Author

René A. J. Janssen − *Molecular Materials and Nanosystems & Institute for Complex Molecular Systems, Eindhoven University of Technology, Eindhoven 5600 MB, The Netherlands; Dutch Institute for Fundamental Energy Research, Eindhoven 5612, The Netherlands;* orcid.org/0000-0002-1920-5124; Email: r.a.j.janssen@tue.nl

Authors

Nick R. M. Schipper − *Molecular Materials and Nanosystems & Institute for Complex Molecular Systems, Eindhoven University of Technology, Eindhoven 5600 MB, The Netherlands*

Guus J. W. Aalbers − *Molecular Materials and Nanosystems & Institute for Complex Molecular Systems, Eindhoven University of Technology, Eindhoven 5600 MB, The Netherlands;* orcid.org/0000-0002-0089-8493

Laura Bellini − *Molecular Materials and Nanosystems & Institute for Complex Molecular Systems, Eindhoven University of Technology, Eindhoven 5600 MB, The Netherlands*

Simon V. Quiroz Monnens − *Molecular Materials and Nanosystems & Institute for Complex Molecular Systems, Eindhoven University of Technology, Eindhoven 5600 MB, The Netherlands*

Lana M. Kessels − *Molecular Materials and Nanosystems & Institute for Complex Molecular Systems, Eindhoven University of Technology, Eindhoven 5600 MB, The Netherlands;* orcid.org/0000-0002-8415-3842

Junke Wang − *Clarendon Laboratory, Department of Physics, University of Oxford, Oxford OX1 3PU, U.K.*

Martijn M. Wienk − *Molecular Materials and Nanosystems & Institute for Complex Molecular Systems, Eindhoven University of Technology, Eindhoven 5600 MB, The Netherlands*

Complete contact information is available at: https://pubs.acs.org/10.1021/acsaem.5c02216

Author Contributions

N.R.M.S. conceptualized the project, did the experiments, and was the main author of the study. Highly sensitive sub-bandgap spectroscopy was conducted by G.J.W.A. XPS and XRD characterizations were performed by L.B. SEM measurements

https://doi.org/10.1021/acsaem.5c02216
ACS Appl. Energy Mater. 2025, 8, 14486−14497

were conducted by S.V.Q.M. and L.M.K. J.W. assisted with outlining and structuring the study and with interpreting results. M.M.W. and R.A.J.J. supervised the project. All authors have contributed to the research and approved the manuscript.

Notes

The authors declare no competing financial interest.

■ ACKNOWLEDGMENTS

We acknowledge funding from HyET Solar B.V, the European Research Council (PERSTACK, Grant Agreement No. 101098168), and The Netherlands Organization for Scientific Research (NWO) (Spinoza Grant).

■ REFERENCES

(1) Kojima, A.; Teshima, K.; Shirai, Y.; Miyasaka, T. Organometal Halide Perovskites as Visible-Light Sensitizers for Photovoltaic Cells. *J. Am. Chem. Soc.* **2009**, *131* (17), 6050−6051.

(2) Green, M. A.; Dunlop, E. D.; Yoshita, M.; Kopidakis, N.; Bothe, K.; Siefer, G.; Hao, X.; Jiang, J. Y. Solar Cell Efficiency Tables (Version 65). *Prog. Photovolt. Res. Appl.* **2025**, *33* (1), 3−15.

(3) Wang, J.; Branco, B.; Remmerswaal, W. H. M.; Hu, S.; Schipper, N. R. M.; Zardetto, V.; Bellini, L.; Daub, N.; Wienk, M. M.; Wakamiya, A.; Snaith, H. J.; Janssen, R. A. J. Performance and stability analysis of all-perovskite tandem photovoltaics in light-driven electrochemical water splitting. *Nat. Commun.* **2025**, *16*, 174.

(4) Shockley, W.; Queisser, H. J. Detailed Balance Limit of Efficiency of p−n Junction Solar Cells. *J. Appl. Phys.* **1961**, *32* (3), 510−519.

(5) Yuan, Y.; Yan, G.; Dreessen, C.; Rudolph, T.; Hülsbeck, M.; Klingebiel, B.; Ye, J.; Rau, U.; Kirchartz, T. Shallow Defects and Variable Photoluminescence Decay Times up to 280 μs in Triple-Cation Perovskites. *Nat. Mater.* **2024**, *23* (3), 391−397.

(6) Shockley, W.; Read, W. T., Jr. Statistics of the Recombinations of Holes and Electrons. *Phys. Rev.* **1952**, *87* (5), 835−842.

(7) Li, C.; Guerrero, A.; Huettner, S.; Bisquert, J. Unravelling the Role of Vacancies in Lead Halide Perovskite through Electrical Switching of Photoluminescence. *Nat. Commun.* **2018**, *9*, 5113.

(8) Zhao, I. Y.; Yavuz, I.; Wang, M.; Weber, M. H.; Xu, M.; Lee, J.-H.; Tan, S.; Huang, T.; Meng, D.; Wang, R.; Xue, J.; Lee, S.-J.; Bae, S.-H.; Zhang, A.; Choi, S.-G.; Yin, Y.; Liu, J.; Han, T.-H.; Shi, Y.; Ma, H.; Yang, W.; Xing, Q.; Zhou, Y.; Shi, P.; Wang, S.; Zhang, E.; Bian, J.; Pan, X.; Park, N.-G.; Lee, J.-W.; Yang, Y. Suppressing ion migration in metal halide perovskite via interstitial doping with a trace amount of multivalent cations. *Nat. Mater.* **2022**, *21* (12), 1396−1402.

(9) Wang, F.; Bai, S.; Tress, W.; Hagfeldt, A.; Gao, F. Defects engineering for high-performance perovskite solar cells. *npj Flexible Electronics* **2018**, *2* (1), 22.

(10) Adhyaksa, G. W. P.; Brittman, S.; Āboliņš, H.; Lof, A.; Li, X.; Keelor, J. D.; Luo, Y.; Duevski, T.; Heeren, R. M. A.; Ellis, S. R.; Fenning, D. P.; Garnett, E. C. Understanding Detrimental and Beneficial Grain Boundary Effects in Halide Perovskites. *Adv. Mater.* **2018**, *30* (52), 1804792.

(11) Datta, K.; van Laar, S. C. W.; Taddei, M.; Hidalgo, J.; Kodalle, T.; Aalbers, G. J. W.; Lai, B.; Li, R.; Tamura, N.; Frencken, J. T. W.; Quiroz Monnens, S. V.; Westbrook, R. J. E.; Graham, D. J.; Sutter-Fella, C. M.; Correa-Baena, J.-P.; Ginger, D. S.; Wienk, M. M.; Janssen, R. A. J. Local Halide Heterogeneity Drives Surface Wrinkling in Mixed-Halide Wide-Bandgap Perovskites. *Nat. Commun.* **2025**, *16*, 1967.

(12) Zhu, C.; Niu, X.; Fu, Y.; Li, N.; Hu, C.; Chen, Y.; He, X.; Na, G.; Liu, P.; Zai, H.; Ge, Y.; Lu, Y.; Ke, X.; Bai, Y.; Yang, S.; Chen, P.; Li, Y.; Sui, M.; Zhang, L.; Zhou, H.; Chen, Q. Strain Engineering in Perovskite Solar Cells and Its Impacts on Carrier Dynamics. *Nat. Commun.* **2019**, *10*, 815.

(13) Chen, J.; Park, N.-G. Materials and Methods for Interface Engineering toward Stable and Efficient Perovskite Solar Cells. *ACS Energy Lett.* **2020**, *5* (8), 2742−2786.

(14) Bush, K. A.; Frohna, K.; Prasanna, R.; Beal, R. E.; Leijtens, T.; Swifter, S. A.; McGehee, M. D.; Hoye, R. L. Z.; Bailie, C. D.; Leijtens, T.; Peters, I. M.; Minichetti, M. C.; Rolston, N.; Prasanna, R.; Sofia, S.; Harwood, D.; Holman, Z. C.; Bent, S. F.; Snaith, H. J.; Buonassisi, T.; Shin, S. S.; McGehee, M. D. Compositional Engineering for Efficient Wide Band Gap Perovskites with Improved Stability to Photoinduced Phase Segregation. *ACS Energy Lett.* **2018**, *3* (2), 428−435.

(15) Pereyra, C.; He, X.; Lira-Cantu, M. Additive Engineering for Stable Halide Perovskite Solar Cells. *J. Energy Chem.* **2021**, *60*, 599−634.

(16) Lee, D.-K.; Park, N.-G. Additive Engineering for Highly Efficient and Stable Perovskite Solar Cells. *Appl. Phys. Rev.* **2023**, *10* (1), 011308.

(17) Lee, D.-N.; Jeon, Y.-S.; Cho, S. C.; Lee, S. U.; Park, N.-G. Additive Engineering in Perovskite Solar Cells: Effect of Basicity of Benzoquinone Additives Controlled by Substituent. *ACS Energy Lett.* **2024**, *9* (8), 4172−4179.

(18) Chen, J.; Sun, X.; Wang, Z.; Cui, X.; Chen, X.; Li, Z.; Feng, X.; Tang, J.; Yang, M.; Yuan, Z.; Zhang, Z.; La, S.; Li, X.; Dai, S.; Cai, M. Rubidium Halide Additive Engineering for Efficient and Stable Bifacial Perovskite Solar Cells. *Adv. Funct. Mater.* **2024**, *35* (3), 2411010.

(19) Nguyen, T. T.; Kim, J.; Kim, Y. S.; Nguyen, B. P.; Jo, W. Wide-Bandgap Perovskites for Multijunction Solar Cells: Improvement of Crystalline Quality of $Cs_{0.1}FA_{0.9}PbI_{1.4}Br_{1.6}$ by Using Lead Thiocyanate. *J. Mater. Chem. A* **2023**, *11* (19), 10254−10266.

(20) Ke, W.; Xiao, C.; Wang, C.; Saparov, B.; Duan, H.-S.; Zhao, D.; Xiao, Z.; Schulz, P.; Harvey, S. P.; Liao, W.; Meng, W.; Yu, Y.; Cimaroli, A. J.; Jiang, C.-S.; Zhu, K.; Al-Jassim, M.; Fang, G.; Mitzi, D. B.; Yan, Y. Employing Lead Thiocyanate Additive To Reduce the Hysteresis and Boost the Fill Factor of Planar Perovskite Solar Cells. *Adv. Mater.* **2016**, *28* (26), 5214−5221.

(21) Heo, D. Y.; Lee, T. H.; Iwan, A.; Kavan, L.; Omatova, M.; Majkova, E.; Kamarás, K.; Jang, H. W.; Kim, S. Y. Effect of Lead Thiocyanate Ions on Performance of Tin-Based Perovskite Solar Cells. *J. Power Sources* **2020**, *458*, 228067.

(22) Pham, N. D.; Tiong, V. T.; Chen, P.; Wang, L.; Wilson, G. J.; Bell, J.; Wang, H. Enhanced Perovskite Electronic Properties via a Modified Lead(II) Chloride Lewis Acid−Base Adduct and Their Effect in High-Efficiency Perovskite Solar Cells. *J. Mater. Chem. A* **2017**, *5* (10), 5195−5203.

(23) Ebadi, M.; Sefidi, P. Y.; Samadifar, A.; Salari, D.; Darbandi, M.; Hosseini, M. G. Influence of Lead (II) Chloride and/or Lead (II) Bromide Entrance on the Efficiency and Stability of Methyl Ammonium Lead Triiodide Perovskite Solar Cell: Comparative Study of the Halide Composition and Substitution Percentage. *Opt. Mater.* **2021**, *113*, 110888.

(24) Zhang, X.; Yang, D.; Yang, R.; Zhu, X.; Feng, J.; Wang, Z.; Zuo, S.; Niu, J.; Liu, S. Exposed the Mechanism of Lead Chloride Dopant for High Efficiency Planar-Structure Perovskite Solar Cells. *Org. Electron.* **2018**, *62*, 499−504.

(25) Wang, J.; Zeng, L.; Zhang, D.; Maxwell, A.; Chen, H.; Datta, K.; Caiazzo, A.; Remmerswaal, W. H. M.; Schipper, N. R. M.; Chen, Z.; Ho, K.; Dasgupta, A.; Kusch, G.; Ollearo, R.; Bellini, L.; Hu, S.; Wang, Z.; Li, C.; Teale, S.; Grater, L.; Chen, B.; Wienk, M. M.; Oliver, R. A.; Snaith, H. J.; Janssen, R. A. J.; Sargent, E. H. Halide Homogenization for Low Energy Loss in 2-eV-Bandgap Perovskites and Increased Efficiency in All-Perovskite Triple-Junction Solar Cells. *Nat. Energy* **2024**, *9* (1), 70−80.

(26) McMeekin, D. P.; Sadoughi, G.; Rehman, W.; Eperon, G. E.; Saliba, M.; Hörantner, M. T.; Haghighirad, A.; Sakai, N.; Korte, L.; Rech, B.; Johnston, M. B.; Herz, L. M.; Snaith, H. J. A Mixed-Cation Lead Mixed-Halide Perovskite Absorber for Tandem Solar Cells. *Science* **2016**, *351* (6269), 151−155.

(27) Tumen-Ulzii, G.; Qin, C.; Klotz, D.; Leyden, M. R.; Wang, P.; Auffray, M.; Fujihara, T.; Matsushima, T.; Lee, J.-W.; Lee, S.-J.; Yang, Y.; Adachi, C. Detrimental Effect of Unreacted PbI_2 on the Long-

https://doi.org/10.1021/acsaem.5c02216
ACS Appl. Energy Mater. 2025, 8, 14486−14497

Term Stability of Perovskite Solar Cells. *Adv. Mater.* **2020**, *32* (16), 1905035.
(28) Lim, E. L.; Wei, Z. A. Short Overview of the Lead Iodide Residue Impact and Regulation Strategies in Perovskite Solar Cells. *J. Energy Chem.* **2024**, *90*, 504−510.
(29) Wang, Z.; Liu, L.; Liu, X.; Song, D.; Shi, D.; Wu, S.; Tong, Y.; Ren, H.; Li, M.; Zheng, Y.; Zhao, D. Uncovering Synergistic Effect of Chloride Additives for Efficient Quasi-2D Perovskite Solar Cells. *Chem. Eng. J.* **2022**, *432*, 134367.
(30) Kubota, S.; Ozaki, S.; Onishi, J.; Kano, K.; Shirai, O. Selectivity on Ion Transport across Bilayer Lipid Membranes in the Presence of Gramicidin A. *Anal. Sci.* **2009**, *25* (2), 189−193.
(31) Daub, M.; Hillebrecht, H. Synthesis, Single-Crystal Structure and Characterization of $(CH_3NH_3)_2Pb(SCN)_2I_2$. *Angew. Chem., Int. Ed.* **2015**, *54* (38), 11016−11017.
(32) Yamamoto, T.; Oswald, I. W. H.; Savory, C. N.; Ohmi, T.; Koegel, A. A.; Scanlon, D. O.; Kageyama, H.; Neilson, J. R. Structure and Optical Properties of Layered Perovskite $(MA)_2PbI_{2-x}Br_x(SCN)_2$ $(0 \leq x < 1.6)$. *Inorg. Chem.* **2020**, *59* (33), 17379−17384.
(33) Ohmi, T.; Miura, T.; Shigematsu, K.; Koegel, A. A.; Newell, B. S.; Neilson, J. R.; Ikoma, T.; Azuma, M.; Yamamoto, T. Temperature-Induced Structural Transition in an Organic−Inorganic Hybrid Layered Perovskite $(MA)_2PbI_{2-x}Br_x(SCN)_2$. *CrystEngComm* **2022**, *24* (30), 5428−5434.
(34) Numata, Y.; Sanehira, Y.; Ishikawa, R.; Shirai, H.; Miyasaka, T. Thiocyanate Containing Two-Dimensional Cesium Lead Iodide Perovskite, $Cs_2PbI_2(SCN)_2$: Characterization, Photovoltaic Application, and Degradation Mechanism. *ACS Appl. Mater. Interfaces* **2018**, *10* (49), 42363−42371.
(35) Ohmi, T.; Oswald, I. W. H.; Neilson, J. R.; Roth, N.; Nishioka, S.; Maeda, K.; Fujii, K.; Yashima, M.; Azuma, M.; Yamamoto, T. Thiocyanate-Stabilized Pseudo-Cubic Perovskite $CH(NH_2)_2PbI_3$ from Coincident Columnar Defect Lattices. *J. Am. Chem. Soc.* **2023**, *145* (36), 19759−19767.
(36) Ohmi, T.; Neilson, J. R.; Taniguchi, W.; Fukui, T.; Nagase, T.; Haruta, Y.; Saidaminov, M. I.; Fukushima, T.; Azuma, M.; Yamamoto, T. $FA_4Pb_2I_{7.5}(SCN)_{05}$: n = 3 Member of Perovskite Homologous Series $FA_{n+1}Pb_{n-1}I_{3n-1.5}(SCN)_{0.5}$ with Columnar Defects. *ACS Mater. Lett.* **2024**, *6* (5), 1913−1919.
(37) Xu, J.; Boyd, C. C.; Yu, Z. J.; Palmstrom, A. F.; Witter, D. J.; Larson, B. W.; France, R. M.; Werner, J.; Harvey, S. P.; Wolf, E. J.; Weigand, W.; Manzoor, S.; van Hest, M. F. A. M.; Berry, J. J.; Luther, J. M.; Holman, Z. C.; McGehee, M. D. Triple-Halide Wide−Band Gap Perovskites with Suppressed Phase Segregation for Efficient Tandems. *Science* **2020**, *367* (6482), 1097−1104.
(38) Pu, Y.; Su, H.; Liu, C.; Guo, M.; Liu, L.; Fu, H. A Review on Buried Interface of Perovskite Solar Cells. *Energies* **2023**, *16* (13), 5015.
(39) Aalbers, G. J. W.; Remmerswaal, W. H. M.; van den Heuvel, R. H. C.; Bellini, L.; Kessels, L. M.; Weijtens, C. H. L.; Schipper, N. R. M.; Wienk, M. M.; Janssen, R. A. J. Functionalized Substrates for Reduced Nonradiative Recombination in Metal-Halide Perovskites. *J. Phys. Chem. Lett.* **2025**, *16* (1), 372−377.
(40) Remmerswaal, W. H. M.; Kessels, L. M.; Branco, B.; van Huisseling, G. G. F.; Zhang, D.; Wienk, M. M.; Janssen, R. A. J. Analysis of interfacial losses and passivation strategies for narrow-bandgap perovskite solar cells. *Sol. RRL* **2025**, *9*, No. e2500291.
(41) Warby, J.; Shah, S.; Thiesbrummel, J.; Gutierrez-Partida, E.; Lai, H.; Alebachew, B.; Grischek, M.; Yang, F.; Lang, F.; Albrecht, S.; Fu, F.; Neher, D.; Stolterfoht, M. Mismatch of Quasi−Fermi Level Splitting and V_{oc} in Perovskite Solar Cells. *Adv. Energy Mater.* **2023**, *13*, 2303135.
(42) Remmerswaal, W. H. M.; van Gorkom, B. T.; Zhang, D.; Wienk, M. M.; Janssen, R. A. J. Quantifying Non-Radiative Recombination in Passivated Wide-Bandgap Metal Halide Perovskites Using Absolute Photoluminescence Spectroscopy. *Adv. Energy Mater.* **2024**, *14* (12), 2303664.
(43) van Gorkom, B. T.; van der Pol, T. P. A.; Datta, K.; Wienk, M. M.; Janssen, R. A. J. Revealing Defective Interfaces in Perovskite Solar Cells from Highly Sensitive Sub-Bandgap Photocurrent Spectroscopy Using Optical Cavities. *Nat. Commun.* **2022**, *13*, 349.
(44) Aalbers, G. J. W.; van der Pol, T. P. A.; Datta, K.; Remmerswaal, W. H. M.; Wienk, M. M.; Janssen, R. A. J. Effect of Sub-Bandgap Defects on Radiative and Non-Radiative Open-Circuit Voltage Losses in Perovskite Solar Cells. *Nat. Commun.* **2024**, *15*, 1276.

https://doi.org/10.1021/acsaem.5c02216
ACS Appl. Energy Mater. 2025, 8, 14486−14497